PARAMETER ESTIMATION
FOR THE FOREST FIRE PROPAGATION MODEL

Martin Ambroz[1] — Karol Mikula[1] — Marek Fraštia[2] —
Marián Marčiš[2]

[1]Department of Mathematics and Descriptive Geometry, Slovak University of Technology
in Bratislava, SLOVAKIA

[2]Department of Surveying, Slovak University of Technology in Bratislava, SLOVAKIA

ABSTRACT. This paper first gives a brief overview of the Lagrangian forest
fire propagation model [Ambroz, M.—Balažovjech, M.—Medľa, M.—Mikula, K.:
*Numerical modeling of wildland surface fire propagation by evolving surface
curves*, Adv. Comput. Math. **45** (2019), no. 2, 1067–1103], which we apply to grass-
field areas. Then, we aim to estimate the optimal model parameters. To achieve
this goal, we use data assimilation of the measured data. From the data, we are
able to estimate the normal velocity of the fire front (rate of spread), dominant
wind direction and selected model parameters. In the data assimilation process,
we use the Hausdorff distance as well as the Mean Hausdorff distance as a crite-
rion. Moreover, we predict the fire propagation in small time intervals.

1. Introduction

Modelling of a forest fire spread is a challenging task since it is a very com-
plex phenomenon. In this paper, we estimate the optimal parameters for the
mathematical model of the forest fire propagation [1] applied on a grassfield.
This empirical mathematical model driving a surface curve considers the het-
erogeneity of fuel burnability, wind speed and direction, terrain slope influence
and the shape of the curve on the terrain. To obtain a reliable output from the
model, we need to find the optimal values of the model parameters. Using data
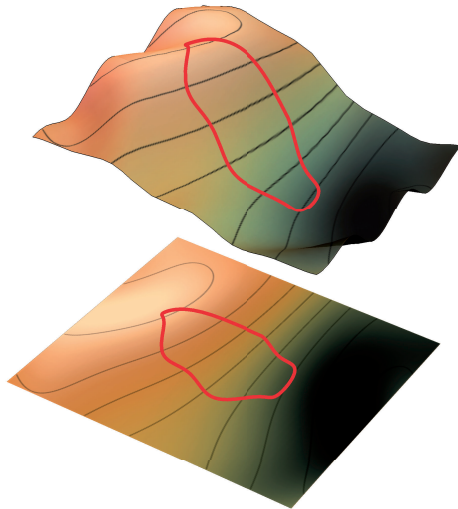assimilation for two grassland fires we look for such optimal values.

FIGURE 1. Surface curve $\mathcal{G}$, for which we design the mathematical model and the projected closed planar curve Γ which is used for numerical computations.

2. Forest fire propagation model

We consider the time evolution of a closed planar curve Γ, which is a projection of a surface curve $\mathcal{G}$, see Fig. 1. The evolution is given by the general equation

$$\frac{\partial \mathbf{x}}{\partial t} = v\left(\mathbf{x}, t\right), \tag{1}$$

where $\mathbf{x}$ is a position vector of the evolving planar curve, t is time, $\frac{\partial \mathbf{x}}{\partial t}$ denotes the speed of the curve motion.

The projected planar curve Γ moves in time by a general planar velocity vector field $v\left(\mathbf{x}, t\right)$. We can split such a general motion of any point $\mathbf{x}$ of the curve Γ into the normal and tangential directions, so we consider a general form of the planar curve evolution in the following form

$$\frac{\partial \mathbf{x}}{\partial t} = \beta \mathbf{N} + \alpha \mathbf{T}, \tag{2}$$

where β is the velocity in the normal direction $\mathbf{N}$ and α is the tangential velocity of the planar curve Γ. While the normal velocity changes the curve shape, the tangential velocity does not in the continuous form. In the discrete form, we use the tangential velocity for the redistribution of curve grid points that stabilizes the numerical model [4, 6].

Note that all the influences to the normal velocity are given for the curve on the surface φ, but the projected planar curve evolution is solved numerically. Thus, we want to relate the normal velocity $\mathcal{V}$ (velocity in the direction of the normal vector $\mathcal{N}$) of the surface curve $\mathcal{G}$ to the normal velocity β of projected curve Γ. Following [5] we get that

$$\mathcal{V} = \mathcal{G}_t \cdot \mathcal{N} = (x_t, y_t, \varphi_t(x,y)) \cdot \mathcal{N} = (\mathbf{x}_t, \mathbf{x}_t \cdot \nabla\varphi) \cdot \mathcal{N}$$
$$= \sqrt{\frac{1 + |\nabla\varphi|^2}{1 + (\nabla\varphi \cdot \mathbf{T})^2}} \beta, \tag{3}$$

from where we obtain

$$\beta = \mathcal{V}\sqrt{\frac{1 + (\nabla\varphi \cdot \mathbf{T})^2}{1 + |\nabla\varphi|^2}}. \tag{4}$$

2.1. Normal velocity of the surface curve

Normal velocity $\mathcal{V}$ of the surface curve $\mathcal{G}$ is given by the external influences, expressed by the external force $\mathcal{F}$, and the local shape of the curve with respect to the topography, which is expressed by the curvatures. The external force $\mathcal{F}$ plays the dominant role in the normal velocity, while the geodesic and normal curvatures can accelerate it or slow it down. Such a normal velocity $\mathcal{V}$ in the outer direction of the curve $\mathcal{G}$ is given by

$$\mathcal{V} = \mathcal{F}\left(\delta_\mathcal{F} - \delta_g K_g + \delta_n K_n\right), \tag{5}$$

where $\delta_\mathcal{F}$ is the weight of the external force, δ_g is the weight of the geodesic curvature and δ_n is the weight of the normal curvature influence on the fire spread. The geodesic curvature in the tangent plane to the surface, K_g, smooths the curve. The normal curvature K_n of the curve evolving in a valley (or on a ridge) can increase (or decrease) the normal velocity $\mathcal{V}$.

Our design of an external force influencing the fire behaviour is based on the empirical laws of the wildland fire perimeter propagation. Research indicates that the wildland fire propagation is influenced by the fuel parameters, weather conditions and surrounding topography slope. Considering the most important factors, we suggest the following formula for the external force

$$\mathcal{F} = f \, f_w(\mathbf{w} \cdot \mathcal{N}) \, f_s(\mathbf{s} \cdot \mathcal{N}), \tag{6}$$

where f is the so-called rate of spread (ROS), $f_w(\mathbf{w} \cdot \mathcal{N})$ is the wind influence and $f_s(\mathbf{s} \cdot \mathcal{N})$ is the terrain slope influence on the rate of spread, with $\mathbf{w}$ being the three dimensional wind vector, $\mathbf{s}$ being the three dimensional slope vector and $\mathcal{N}$ being the unit normal vector in the tangent plane to the surface curve.

A surface fuel is usually not homogeneous and therefore we assume a heterogeneous fuel flammability on a topographic surface. Therefore, the spatial variability in ROS is expressed by a 2-D ROS map, $f(\mathbf{x})$, $\mathbf{x} \in \Omega \subset \mathbb{R}^2$, $f(\mathbf{x})$ gives the rate of spread in a point $(\mathbf{x}_i, \varphi(\mathbf{x}_i))$ on the surface.

The topography slope increases the radiation and convection heat transfer up the slope and thus accelerates or slows down the fire spread, see Fig. 2 left. From the digital terrain model (the topography function φ) we can easily obtain a vector function $\nabla\varphi$ characterizing the topography slope. Now, we adjust 2D vector function $\nabla\varphi$ to the tangent plane to get a slope vector $\mathbf{s}$. According to [11], the slope influences the rate of spread exponentially, depending on the projection of $\mathbf{s}$ to $\mathcal{N}$, therefore we consider

$$f_s(\mathbf{s} \cdot \mathcal{N}) = e^{\lambda_s(\mathbf{s} \cdot \mathcal{N})}, \tag{7}$$

where λ_s is a positive parameter.

According to [11] the wind influences the rate of spread exponentially, so we consider the scalar product of the wind vector $\mathbf{w}$ and the outer normal vector $\mathcal{N}$ as an exponent of the function f_w in the form

$$f_w(\mathbf{w} \cdot \mathcal{N}) = e^{\lambda_w(\mathbf{w} \cdot \mathcal{N})}, \tag{8}$$

where λ_w is a positive parameter. If those vectors are perpendicular, $\mathbf{w} \cdot \mathcal{N} = 0$, the external force $\mathcal{F}$ is not influenced by the wind, because $f_w = 1$. If the vectors are parallel, with the same orientation, $\mathbf{w} \cdot \mathcal{N} = |\mathbf{w}|$, $f_w = e^{\lambda_w |\mathbf{w}|}$, the influence of the wind is the strongest, see Fig. 2 center and right.
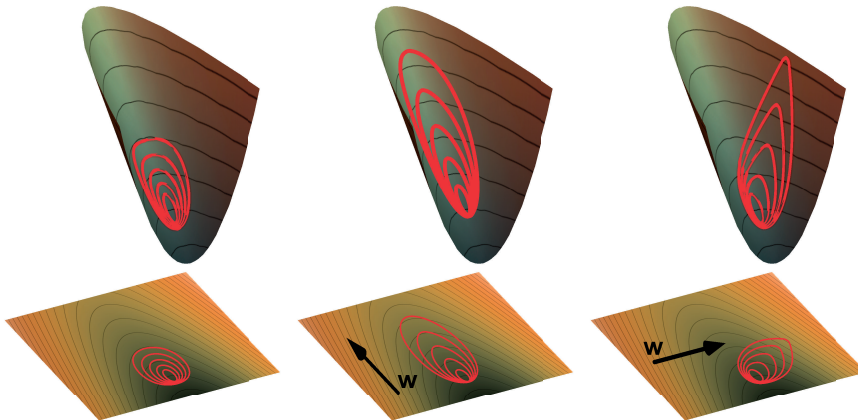

FIGURE 2. Visualization of slope and wind influences on a simple topography. Left: rising terrain slope increases the fire spread while descending terrain slope slows the fire spread down. Center and right: wind direction, given by vector $\mathbf{w}$, increases the fire spread in the same direction while in the opposite direction, the wind slows the fire spread down.

3. Evolution algorithm

Curve Γ is a close plane curve, $\Gamma : S^1 \to \mathbf{R}^2$, parametrized by $u \in S^1$, where S^1 is a circle with unit length, thus $u \in [0, 1]$ and $\Gamma = \{\mathbf{x}(u), u \in S^1\}$, where $\mathbf{x}(u) = (\mathbf{x}_1(u), \mathbf{x}_2(u))$ is the position vector of the curve Γ for parameter u. In the sequel, the curve will be discretized to a set of points. An example of a closed planar curve discretization is displayed in Fig. 3, where $\mathbf{x}_0, \mathbf{x}_1, \ldots, \mathbf{x}_n$ are discrete curve points which correspond to the uniform discretization of the unit circle with step $h = 1/n$ and $\mathbf{x}_0 = \mathbf{x}_n$.
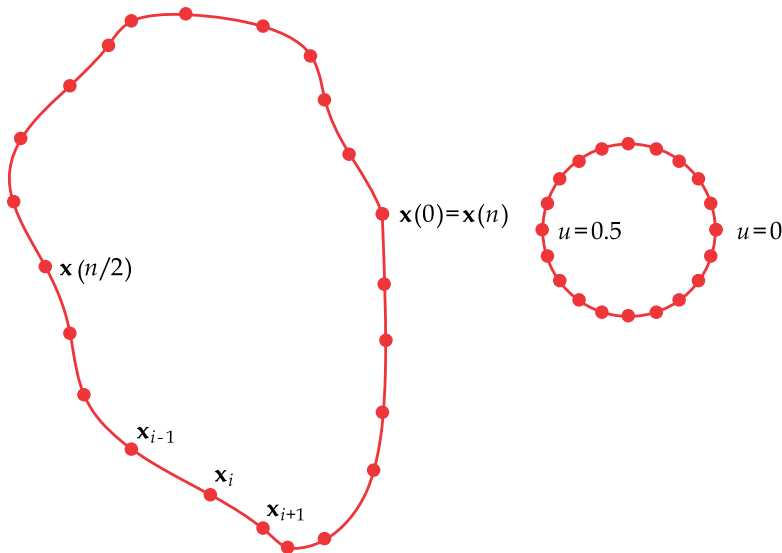

FIGURE 3. Closed planar curve discretization (left) corresponding to uniform discretization of the unit circle (right) [1].

Let $|\mathbf{x}_u| > 0$, where $\mathbf{x}_u = \left(\frac{\partial \mathbf{x}_1}{\partial u}, \frac{\partial \mathbf{x}_2}{\partial u}\right)$ and $g = |\mathbf{x}_u| = \sqrt{\left(\frac{\partial \mathbf{x}_1}{\partial u}\right)^2 + \left(\frac{\partial \mathbf{x}_2}{\partial u}\right)^2}$. Let us denote by s the unit arc-length parametrization of the curve Γ. Then $ds = |\mathbf{x}_u|du = gdu$ and $du = \frac{1}{g}ds$. If the curve Γ is parametrized in a counterclockwise direction, the unique definition of the unit tangent $\mathbf{T}$ and (outer) normal $\mathbf{N}$ vectors to the curve Γ can be done as follows: $\mathbf{T} = \frac{\partial \mathbf{x}}{\partial s}$ (denoted also by $\mathbf{x}_s$), $\mathbf{N} = \mathbf{x}_s^{\perp}$ and $\mathbf{T} \wedge \mathbf{N} = -1$, where $\mathbf{T} \wedge \mathbf{N}$ denotes the determinant of the matrix with columns $\mathbf{T}$ and $\mathbf{N}$. If $\mathbf{T} = (\mathbf{x}_{1s}, \mathbf{x}_{2s})$, then $\mathbf{N} = (\mathbf{x}_{2s}, -\mathbf{x}_{1s})$.

Since we consider outer normal, from the Frenet-Serret formulas we have

$$\mathbf{T}_s = -k\mathbf{N} \quad \text{and} \quad \mathbf{N}_s = k\mathbf{T},$$

where k is the curvature. From there it follows that $-k\mathbf{N} = \mathbf{T}_s = (\mathbf{x}_s)_s = \mathbf{x}_{ss}$.

In our approach, the curve Γ is given by its position vector $\mathbf{x}$, so its evolution can be described by the evolution of this vector in time. We consider the general form of the curve evolution (2) where $\beta = w - \varepsilon k$ with

$$\varepsilon = \frac{\mathcal{F}\delta_g}{1 + (\nabla\varphi \cdot \mathbf{T})^2}, \tag{9}$$

$$w = \mathcal{F}\left(\delta_{\mathcal{F}}\sqrt{\frac{1 + (\nabla\varphi \cdot \mathbf{T})^2}{1 + |\nabla\varphi|^2}} + \delta_g \frac{\mathbf{T}^T H(\varphi) \mathbf{T}(\nabla\varphi \cdot \mathbf{N})}{\left(1 + (\nabla\varphi \cdot \mathbf{T})^2\right)\left(1 + |\nabla\varphi|^2\right)} + \right.$$
$$\left. \delta_n \frac{\mathbf{T}^T H(\varphi) \mathbf{T}}{\sqrt{1 + (\nabla\varphi \cdot \mathbf{T})^2 \left(1 + |\nabla\varphi|^2\right)}}\right), \tag{10}$$

where $H(\varphi)$ is the square matrix of the second-order partial derivatives of the topography function φ.

Then using the Frenet-Serret formula, mentioned above, we can rewrite (2) into the form of the so-called intrinsic partial differential equation

$$\mathbf{x}_t = (w - \delta k)\mathbf{N} + \alpha\mathbf{T} = w\mathbf{N} - \delta k\mathbf{N} + \alpha\mathbf{T} = \delta\mathbf{x}_{ss} + \alpha\mathbf{x}_s + w\mathbf{x}_s^\perp \tag{11}$$

which is suitable for numerical discretization. Since $\mathbf{x} = (\mathbf{x}_1, \mathbf{x}_2)$, (11) represents a system of two partial differential equations for components $\mathbf{x}_1$ and $\mathbf{x}_2$ of the curve position vector $\mathbf{x}$. These two equations are coupled together by the derivatives with respect to the arc-length parametrisation s, because both components of the position vector $\mathbf{x}$ occur in the term ds. The curvature term yields the so-called intrinsic diffusion along the curve (the term $\mathbf{x}_{ss}$), the tangential velocity yields the so-called intrinsic advection along the curve (the term $\mathbf{x}_s$) and the external driving force in the normal direction is given by the third term on the right-hand side of (11).

Using the flowing finite volume method, we get the system of linear equations, which are strictly diagonally dominant, thus it is always solvable by the efficient cyclic tridiagonal solver (a modification of the Thomas algorithm).

4. Numerical experiments

Two fires, see Fig. 4 and 5, were set as a training of the fire-fighting units. The first fire is quite simple. It starts from a small circle and burns along the non-burnable area boundary, see Fig. 4. The dominant spread direction was determined by the direction of the west wind. The second fire was also started from a small circle. However, after some time, another small fire started nearby and it provided us the opportunity to reconstruct the merging fires. There was also a small non-burnable area that split the curve.

FIGURE 4. Image data from quadcopter. Propagation of the first fire perimeter used in the following experiments.

The whole area and fire progress were documented by the quadcopter. Its images were used for the extraction of the fire perimeter evolution in time and the creation of the ROS map. To do so, the technology of the photogrammetry [12] has been used. First, the digital elevation model was generated from drone images by the method of Structure from Motion [2] and then, individual images were redrawing to the reference projection plane [10]. These georeferenced orthoimages have been primary output for the next numerical modelling. Then, the fire perimeters in 2 seconds interval were segmented using the semi-automatic or automatic segmentation algorithms [7,8], see Fig. 6.

FIGURE 5. Image data from quadcopter. Propagation of the second fire perimeter used in the following experiments.
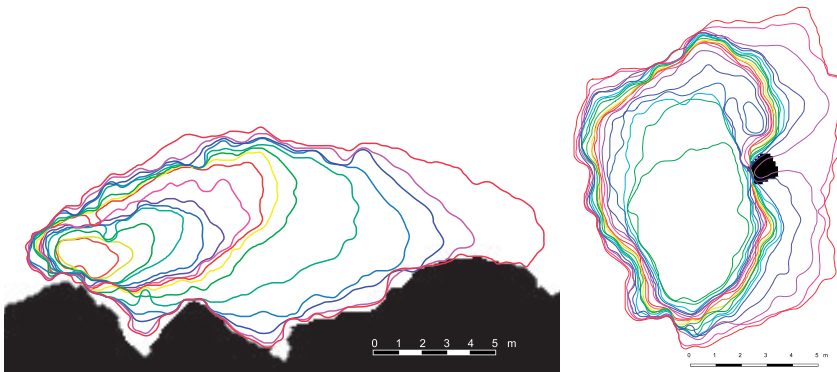

FIGURE 6. Segmented fire perimeter evolution of both experimental fires. Perimeters are plotted over the rate of spread map with the non-burnable areas (black) with no normal velocity and burnable areas (white) where we use the normal velocity estimated in Section 2.1.

To measure the difference between two curves, numerically computed and segmented, we use the Hausdorff distance (HD) as well as the Mean Hausdorff distance (MHD) [3, 13]. The HD between two point sets $A = \{a_1, \ldots, a_{n_A}\}$ and $B = \{b_1, \ldots, b_{n_B}\}$ is defined by the following formula

$$\mathrm{HD}\,(A, B) = \max\left(\mathrm{hd}\,(A, B), \mathrm{hd}\,(B, A)\right), \tag{12}$$

where the so-called directed Hausdorff distance $\mathrm{hd}\,(A, B)$ is given by

$$\mathrm{hd}\,(A, B) = \max_{a_i}\left(\min_{\widehat{b}}\left\|a_i - \widehat{b}\right\|\right), \tag{13}$$

where a_i is the i-th point from the point set A and $\widehat{b}$ is the linear segment between two neighbouring points from the point set B.

The MHD between two point sets $A = \{a_1, \ldots, a_{n_A}\}$ and $B = \{b_1, \ldots, b_{n_B}\}$ is defined by the following formula

$$\mathrm{MHD}\,(A, B) = \max\left(\mathrm{mhd}\,(A, B), \mathrm{mhd}\,(B, A)\right), \tag{14}$$

where the so-called Mean directed Hausdorff distance $\mathrm{mhd}\,(A, B)$ is given by

$$\mathrm{mhd}\,(A, B) = \frac{1}{n_A}\sum_{i=1}^{n_A}\min_{\widehat{b}}\left\|a_i - \widehat{b}\right\|. \tag{15}$$

In the following subsections, we present our approach to the estimation of the model parameters, the wind direction and the rate of spread as well as the model ability to predict the fire evolution. To do so, we use the segmented fire perimeters, which we consider to be the "ground truth". In both experiments, model parameter estimation and prediction of the evolution, we use data assimilation. However, in the model parameter estimation we are only looking for the optimal parameters value, while in the prediction we also update the initial curve.

4.1. Normal velocity estimation

The grassland fires normal velocity (rate of spread - ROS) varies from 0.5 to 1.7 $m \cdot min^{-1}$ in the literature [9]. However, we use observed data for the estimation of the normal velocity. To find the ROS, let us consider the time period (T_1, T_2) with nearly constant wind direction. As we explained in section 2.1, there is no wind influence in the parts of the fire perimeter, that are parallel to the wind direction. Let Γ_1 be a curve at time T_1 and Γ_2 a curve at time T_2 with the number of points n_1, n_2, respectively. Let us define an index set

$$I = \{1, \ldots, n\,(T_1, T_2)\}, \quad \text{where} \quad i \in I$$

if

$$\left|(\Gamma_2)_i - (\Gamma_1)_i\right| > \overline{d}, \overline{d} = \frac{1}{n_1}\sum_{i=1}^{n_1}\left((\Gamma_2)_i - (\Gamma_1)_i\right).$$

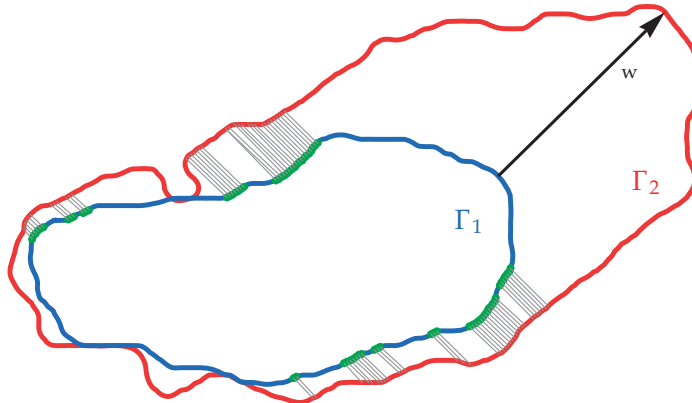MARTIN AMBROZ — KAROL MIKULA — MAREK FRAŠTIA — MARIÁN MARČIŠ

FIGURE 7. Normal velocity estimation. We illustrate the estimated wind direction $\mathbf{w}$ in the time interval (T_1, T_2) and points (green) with tangent almost parallel to $\mathbf{w}$. We also visualize their perpendicular distances (grey) from the points to the curve Γ_2, which we use to compute the normal velocity using (16).

Then we define the wind direction vector

$$\mathbf{w} = \frac{1}{n(T_1, T_2)} \sum_{i \in I} \big((\Gamma_2)_i - (\Gamma_1)_i \big),$$

see Figure 7 as a dominant wind direction from the observed data.

ROS will be computed from the parts of the curve Γ_1, that are almost parallel to the wind direction, i.e., from the points fulfilling $\angle(\mathbf{w}, \mathbf{T}_i) < threshold$, where $\mathbf{T}_i$ is the tangent vector in the point $(\Gamma_1)_i$. For those points we compute the average distance $\overline{D}$ to the curve Γ_2 in perpendicular direction to the wind vector $\mathbf{w}$. Then, measuring time interval in seconds, the estimated value of ROS is given by the function f (in $m \cdot min^{-1}$) as follows

$$f = \frac{60 \, \overline{D}}{T_2 - T_1}. \tag{16}$$

4.2. Model parameter estimation

In the data assimilation process, we vary selected parameters of our model to find the best possible fit between the numerically evolved curve and the corresponding segmented curve, which we consider to be our "ground truth". To get the smallest possible HD or MHD we need to find the optimal values for the parameters λ_w and δ_g. Since the wind direction was not constant throughout the fire propagation, we also vary the wind direction around the estimated $\mathbf{w}$.

10

The other parameters λ_s, δ_n are not included in the data assimilation since the terrain was nearly flat, thus the final formula for the normal velocity $\mathcal{V}$ used in this experiment is

$$\mathcal{V} = f \, e^{\lambda_w} \, (\delta_{\mathcal{F}} - \delta_g K_g) \,, \tag{17}$$

where $\delta_{\mathcal{F}} = 1$.

The initial condition is given by the segmented curve at the time = 0 s. This curve is numerically evolved for 2 (or 4) seconds time interval and is compared to the corresponding segmented curve. This evolution is done for every chosen combination of parameter values and wind direction. The evolution in the next time interval begins from the curve with the best HD or MHD. The parameter values resulting in the best results are presented in Table 1 for MHD and in Table 2 for HD. Together with HD and MHD we present also their relative versions E (in %) with respect to curve perimeter L.

Visual comparison of the curve evolution using the optimal parameters and the real fire position is shown in Figures 8 and 9. Although the MHD, HD and E in Tables 1 and 2 are quite similar, visually it is obvious that the data assimilated curves are the nearest to the real fire position when the time intervals are 2 seconds.

Table 1: The overview of the model parameters λ_w, δ_g, the Mean Hausdorff distance (MHD) between the numerically computed curves and the real fire position and the error (E=MHD/L, where L is the perimeter) in 2–s (columns 2–5) and 4-s time intervals (columns 6–9).

Time	2-s intervals				4-s intervals			
	λ_w	δ_g	MHD	E	λ_w	δ_g	MHD	E
[s]	[−]	[−]	[m]	[%]	[−]	[−]	[m]	[%]
0–2	0.006	0.9	0.038	0.55	0.007	1.2	0.071	1.01
2–4	0.008	1.3	0.071	1.01				
4–6	0.009	0.9	0.107	1.50	0.009	0.9	0.082	1.05
6–8	0.009	0.9	0.082	1.06				
8–10	0.012	1.2	0.079	0.93	0.008	0.9	0.074	0.83
10–12	0.003	1.3	0.074	0.83				
12–14	0.015	1.2	0.099	0.98	0.015	1.3	0.112	1.01
14–16	0.003	0.9	0.151	1.36				
16–18	0.015	1.1	0.145	1.19	0.012	1.3	0.146	1.12
18–20	0.013	1.1	0.138	1.06				
20–22	0.014	1.3	0.162	1.12	0.014	0.9	0.196	1.26
22–24	0.011	0.9	0.199	1.28				
24–26	0.014	1.3	0.139	0.91	0.011	1.3	0.143	0.91
26–28	0.008	1.3	0.145	0.92				

Table 1 Continued

28–30	0.012	0.9	0.142	0.87	0.011	1.3	0.140	0.85
30–32	0.003	0.9	0.148	0.90				
32–34	0.008	1.3	0.156	0.90	0.007	1.1	0.147	0.82
34–36	0.009	1.3	0.152	0.85				
36–38	0.004	0.9	0.159	0.87	0.015	0.9	0.161	0.86
38–40	0.015	1.1	0.159	0.84				
40–42	0.006	0.9	0.205	1.07	0.003	1.3	0.200	1.02
42–44	0.003	0.9	0.204	1.04				
44–46	0.008	1.3	0.217	1.05	0.015	0.9	0.209	0.93
46–48	0.015	1.3	0.220	0.97				
48–50	0.015	0.9	0.229	0.96	0.015	1.3	0.211	0.86
50–52	0.012	1.3	0.208	0.85				
52–54	0.006	1.3	0.202	0.82	0.003	1.3	0.207	0.82
54–56	0.009	1.3	0.174	0.68				
56–58	0.013	1.0	0.170	0.69	0.013	0.9	0.156	0.63
58–60	0.003	0.9	0.182	0.73				
60–62	0.003	1.3	0.165	0.64	0.003	1.3	0.173	0.66
62–64	0.006	1.2	0.169	0.65				
64–66	0.003	1.3	0.186	0.70	0.005	0.9	0.194	0.72
66–68	0.008	1.3	0.197	0.73				
68–70	0.008	1.3	0.206	0.74	0.007	1.3	0.197	0.69
70–72	0.010	1.3	0.198	0.70				
72–74	0.014	1.3	0.181	0.60	0.013	1.3	0.201	0.63
74–76	0.012	1.3	0.194	0.61				
76–78	0.015	0.9	0.230	0.70	0.014	1.0	0.185	0.54
78–80	0.015	1.3	0.216	0.63				
80–82	0.014	1.1	0.202	0.59	0.015	1.2	0.217	0.59
82–84	0.015	1.3	0.188	0.51				
84–86	0.012	1.3	0.198	0.52	0.015	1.3	0.249	0.63
86–88	0.015	1.0	0.203	0.51				
88–90	0.015	0.9	0.263	0.62	0.012	1.3	0.247	0.58
90–92	0.012	1.2	0.249	0.59				
92–94	0.009	0.9	0.222	0.51	0.012	1.1	0.194	0.45
94–96	0.009	0.9	0.208	0.48				
96–98	0.011	0.9	0.221	0.50	0.011	0.9	0.214	0.47
98–100	0.015	1.1	0.222	0.49				

Table 2: The overview of the model parameters λ_w, δ_g, the Hausdorff distance (HD) between numerically computed curves and the real fire position and the error (E=HD/L, where L is the perimeter) in 2–s (columns 2–5) and 4–s time intervals (columns 6–9).

Time	2–s intervals				4–s intervals			
	λ_w	δ_g	HD	E	λ_w	δ_g	HD	E
[s]	[−]	[−]	[m]	[%]	[−]	[−]	[m]	[%]
0–2	0.016	0.9	0.115	1.66	0.015	1.3	0.240	3.47
2–4	0.016	0.9	0.240	3.44				
4–6	0.026	1.3	0.397	5.67	0.022	1.3	0.206	2.94
6–8	0.024	1.3	0.440	6.18				
8–10	0.016	0.9	0.375	4.81	0.030	1.1	0.176	2.26
10–12	0.017	1.0	0.395	4.65				
12–14	0.023	0.9	0.399	4.45	0.028	1.3	0.395	4.41
14–16	0.022	1.3	0.413	4.09				
16–18	0.028	1.3	0.472	4.26	0.028	1.3	0.427	3.85
18–20	0.027	1.0	0.429	3.53				
20–22	0.022	0.9	0.607	4.64	0.027	1.2	0.735	5.62
22–24	0.022	1.0	0.737	5.10				
24–26	0.023	0.9	0.419	2.69	0.020	1.3	0.345	2.22
26–28	0.011	1.3	0.360	2.34				
28–30	0.025	1.2	0.345	2.19	0.023	1.3	0.494	3.14
30–32	0.014	1.0	0.353	2.17				
32–34	0.017	0.9	0.464	2.81	0.021	1.1	0.539	3.27
34–36	0.013	0.9	0.512	2.96				
36–38	0.024	0.9	0.506	2.82	0.022	1.3	0.555	3.10
38–40	0.011	0.9	0.532	2.90				
40–42	0.025	1.0	0.530	2.81	0.005	1.3	0.621	3.29
42–44	0.011	0.9	0.531	2.77				
44–46	0.020	1.2	0.588	3.00	0.024	0.9	0.648	3.32
46–48	0.028	1.0	0.556	2.68				
48–50	0.028	1.3	0.808	3.59	0.030	1.2	0.569	2.53
50–52	0.028	1.1	0.714	2.98				
52–54	0.026	1.2	0.676	2.77	0.029	0.9	0.707	2.89
54–56	0.028	0.9	0.678	2.74				

Table 2 Continued

56–58	0.022	0.9	0.657	2.59	0.020	1.0	0.730	2.87
58–60	0.005	0.9	0.695	2.82				
60–62	0.020	0.9	0.796	3.20	0.026	1.3	0.841	3.38
62–64	0.028	1.3	0.706	2.76				
64–66	0.016	0.9	0.814	3.12	0.021	0.9	0.872	3.35
66–68	0.016	1.3	0.824	3.09				
68–70	0.016	0.9	0.880	3.26	0.019	0.9	0.823	3.05
70–72	0.010	0.9	0.884	3.19				
72–74	0.022	0.9	0.890	3.14	0.027	0.9	0.957	3.38
74–76	0.028	1.3	0.866	2.85				
76–78	0.027	1.3	0.895	2.80	0.023	1.3	0.724	2.27
78–80	0.028	1.3	0.896	2.71				
80–82	0.028	0.9	0.981	2.87	0.027	0.9	0.459	1.34
82–84	0.019	1.3	0.904	2.64				
84–86	0.023	1.3	0.922	2.51	0.019	1.3	0.150	0.41
86–88	0.023	1.3	0.136	0.36				
88–90	0.032	1.1	0.376	0.95	0.028	0.9	0.286	0.72
90–92	0.032	0.9	0.210	0.49				
92–94	0.032	1.2	0.167	0.39	0.028	0.9	0.295	0.69
94–96	0.031	1.1	0.144	0.33				
96–98	0.032	1.1	0.211	0.49	0.028	0.9	0.469	1.08
98–100	0.032	1.0	0.331	0.74				

4.3. Prediction of the evolution

In this experiment, we use the data assimilation results to predict the fire evolution. The basic idea of our prediction is that we evolve the curve (given by the current observed fire front position) using the parameters obtained from data assimilation in the previous time interval. It means, we predict the fire position in time $t+\epsilon$, using the observed fire position at time t and the parameters used in the data assimilation at time interval $(t - \epsilon, t)$.

We visually compare the predictions to the best possible fit on Figures 10--11 for the first fire and Figures 12–13 for the second fire. The best possible fit is found using the data assimilation in time interval $(t, t + \epsilon)$, with the initial condition given by the curve segmented in time t and the "ground truth" is the segmented curve at the time $t + \epsilon$.
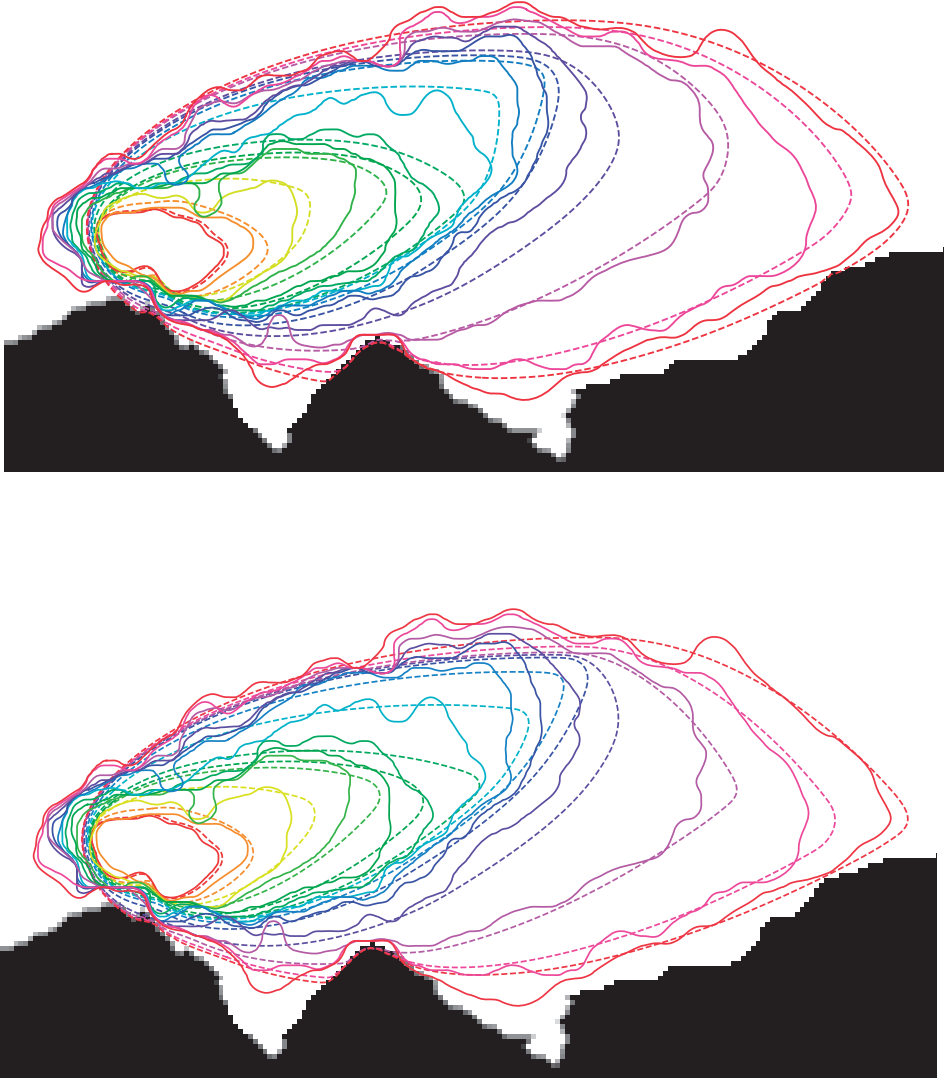
FIGURE 8. Visual comparison of numerically computed curves (dashed) and real fire positions (solid curves). Numerical solution is the best possible fit with respect to the MHD. The time intervals were 2 seconds on the upper image and 4 seconds on the bottom image, see also Table 1.
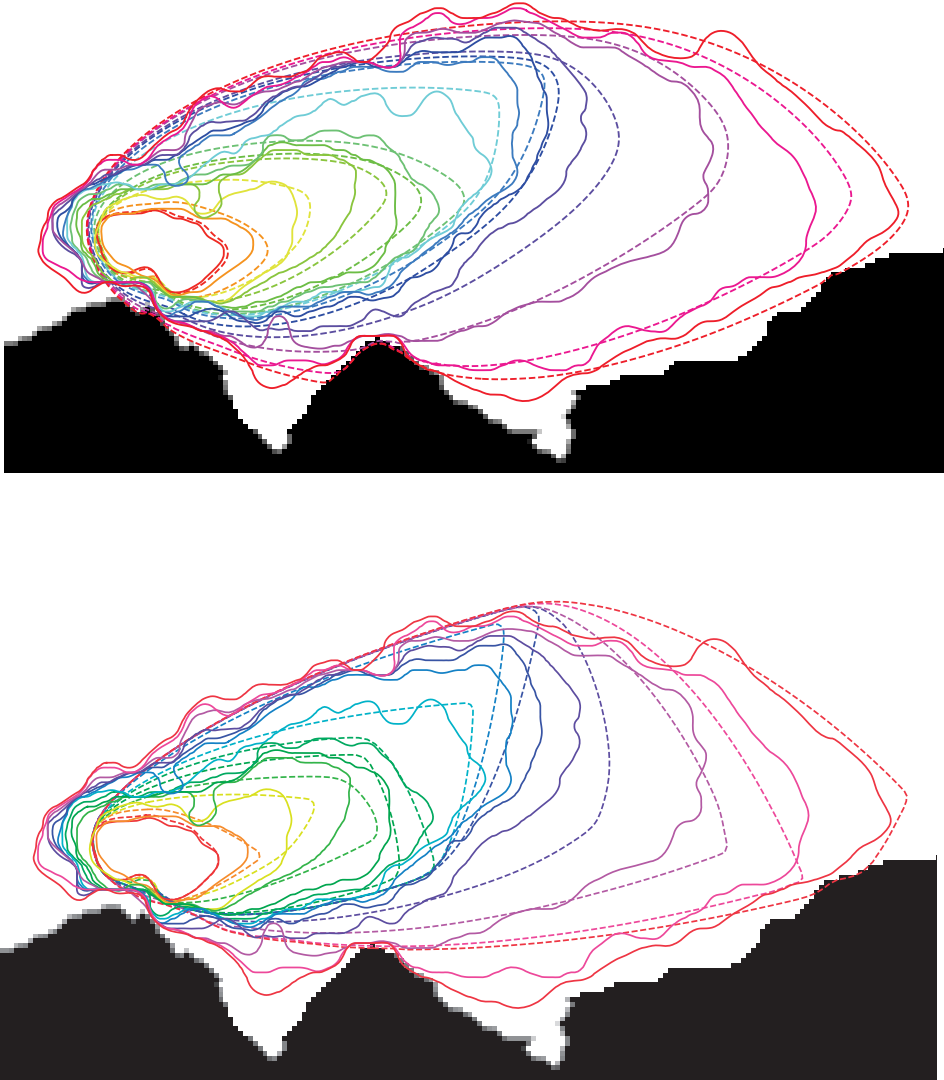
FIGURE 9. Visual comparison of numerically computed curves (dashed) and real fire positions (solid curves). Numerical solution is the best possible fit with respect to the HD. The time intervals were 2 seconds on the upper image and 4 seconds on the bottom image, see also Table 2.
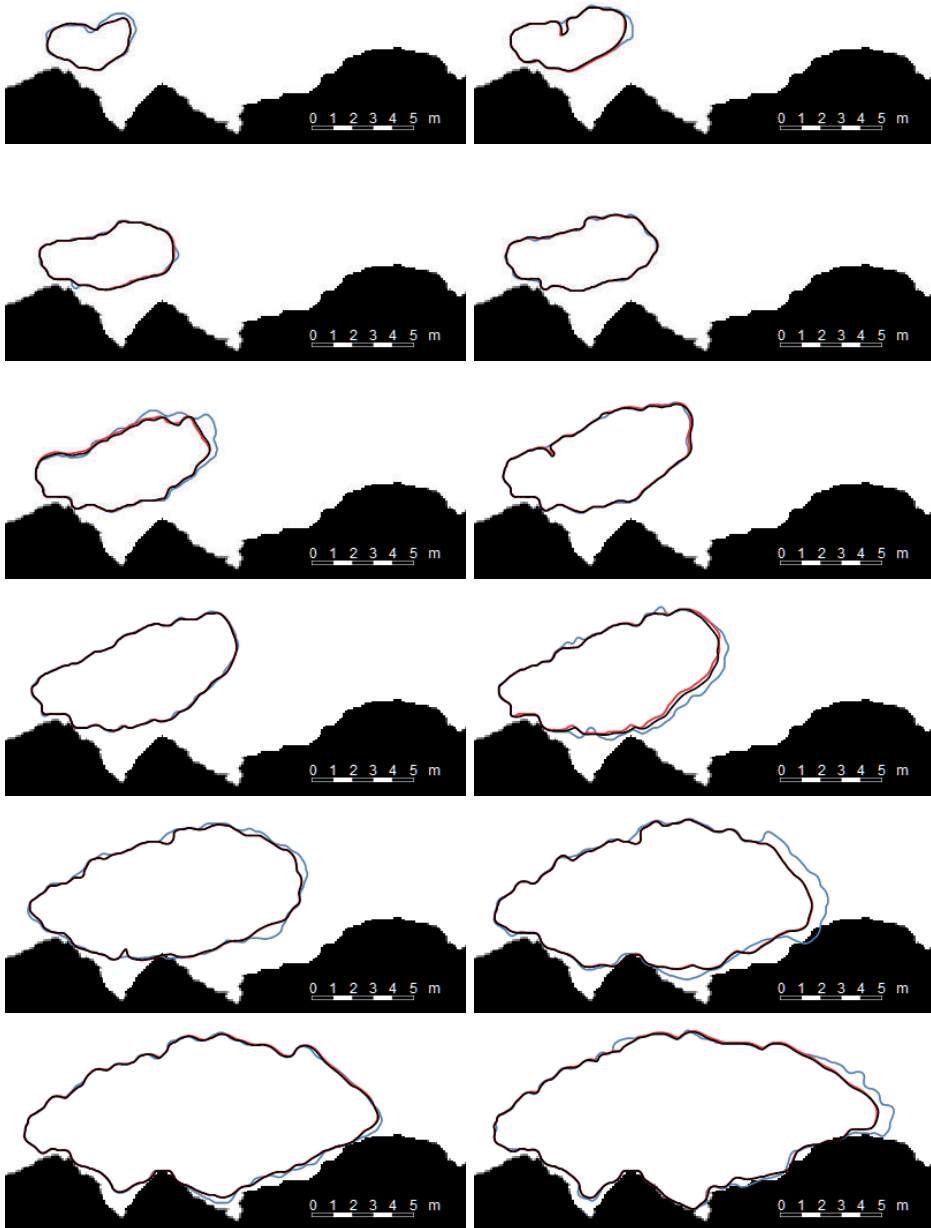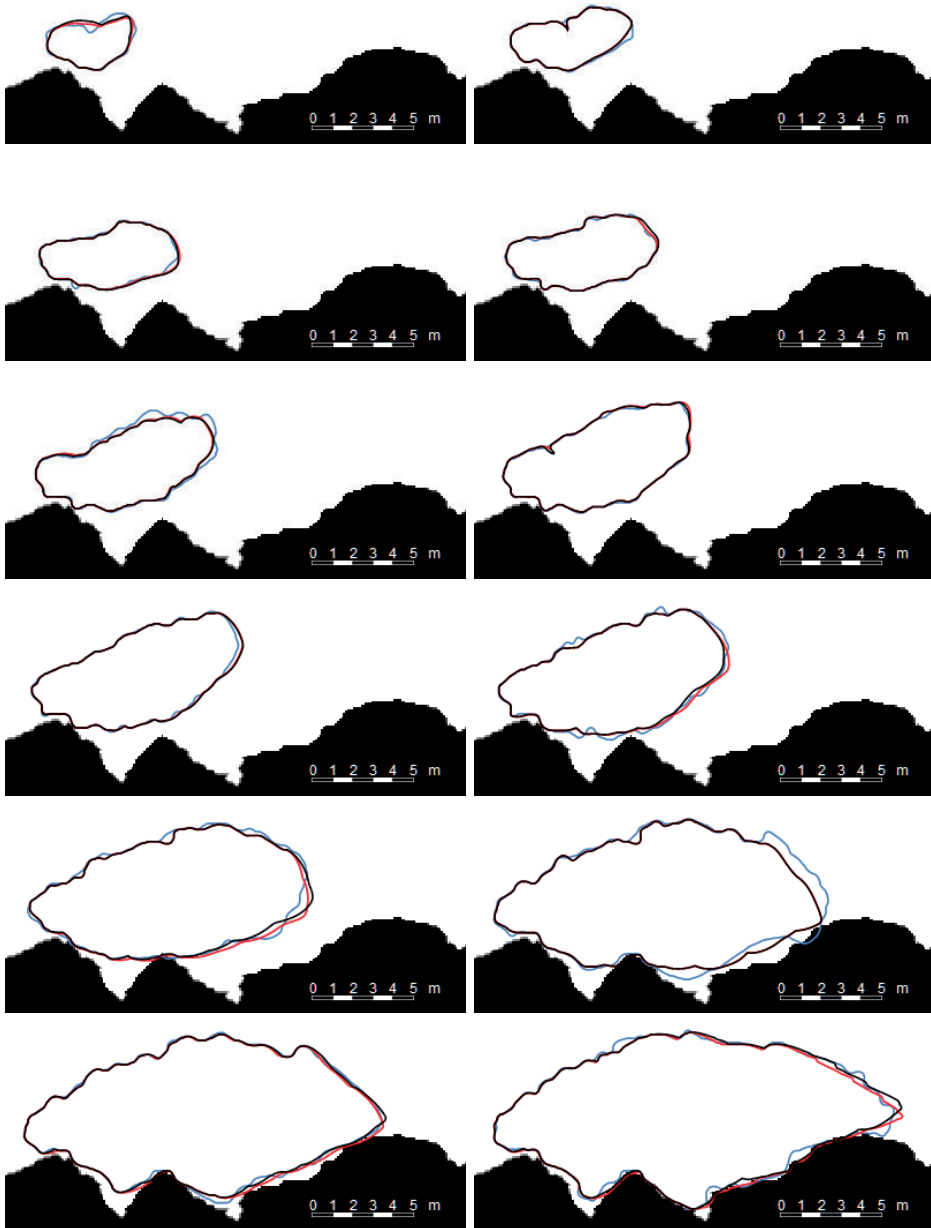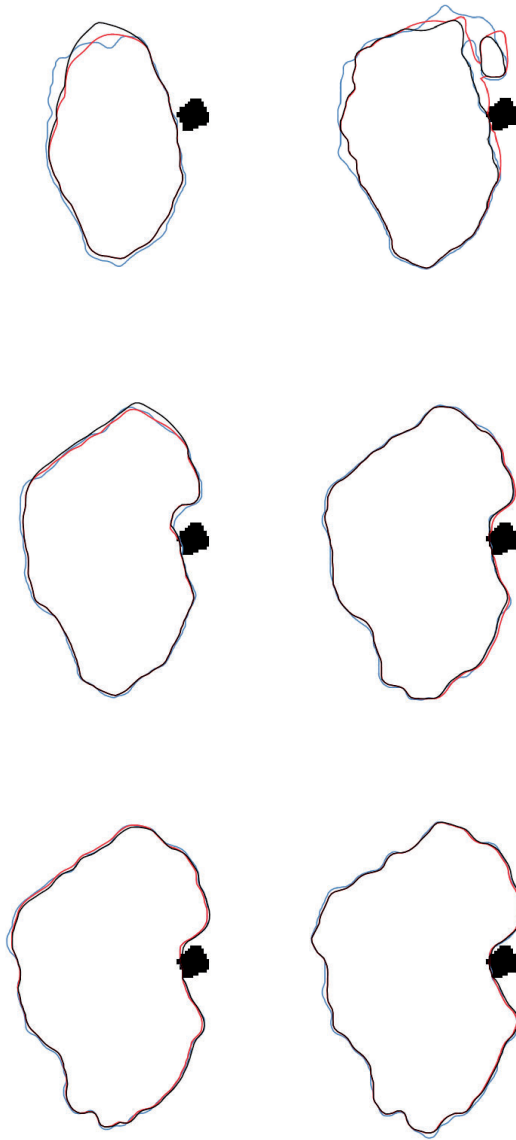
FIGURE 10. Prediction (black) of a fire evolution compared to the best possible fit (red) and the real fire position (blue). Parameters used in the predictions come from the data assimilation from the previous time interval with the Mean Hausdorff distance (MHD) as a criterion.

FIGURE 11. Prediction (black) of a fire evolution compared to the best possible fit (red) and the real fire position (blue). Parameters used in the predictions come from the data assimilation from the previous time interval with the Hausdorff distance (HD) as a criterion.

FIGURE 12. Prediction (black) of a fire evolution compared to the best possible fit (red) and the real fire position (blue). Parameters used in the predictions come from the data assimilation from the previous time interval with the Mean Hausdorff distance (MHD) as a criterion.
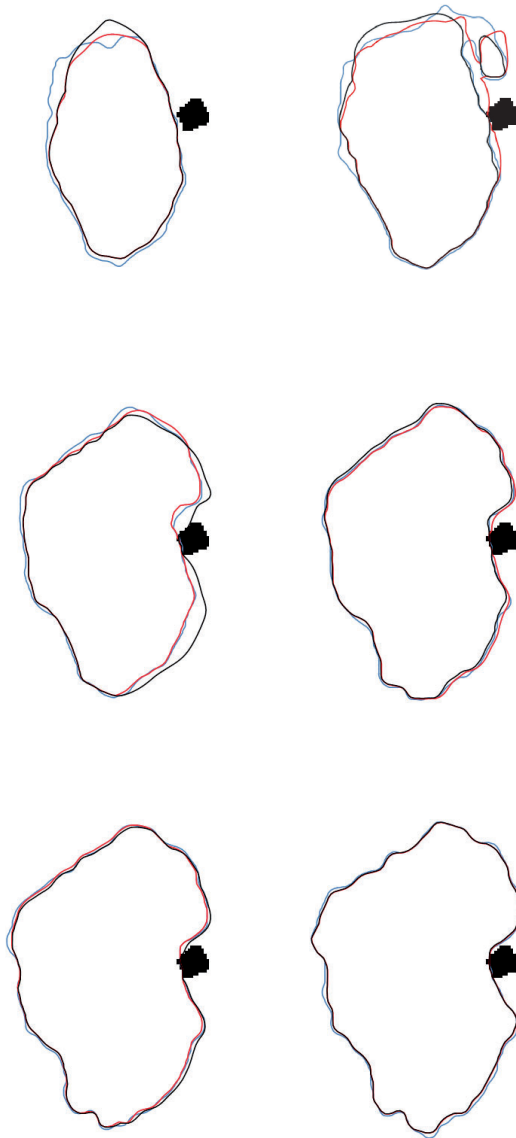
FIGURE 13. Prediction (black) of a fire evolution compared to the best possible fit (red) and the real fire position (blue). Parameters used in the predictions come from the data assimilation from the previous time interval with the Hausdorff distance (HD) as a criterion.

5. Conclusions

In this paper, we presented data assimilation in the forest fire propagation model [1]. Model parameter estimation (MPE) showed, that our model is able to reconstruct fires accurately, i.e., the Mean Hausdorff distance was mostly below 1 % of the fire perimeter length and the Hausdorff distance was mostly below 5 % of the fire perimeter length using 2 second time interval. Besides that, the output from the MPE is valuable as a reference value for the further use of the model. One of the possible applications is also in the fire propagation prediction. In the presented MPE and fire predictions we used the Hausdorff distance as well as the Mean Hausdorff distance as a criterion. Presented results showed better prediction performance of the model with the Hausdorff distance used as a criterion.

REFERENCES

[1] AMBROZ, M.—BALAŽOVJECH, M.—MEDĽA, M.—MIKULA, K.: *Numerical modeling of wildland surface fire propagation by evolving surface curves*, Adv. Comput. Math., **45** (2019), no. 2, 1067–1103.

[2] CIPOLLA, R.: *Structure from motion*, 2008. Available online at: `http://mi.eng.cam.ac.uk/$\sim$cipolla/publications/contributionToEditedBook/2008-SFM-chapters.pdf`

[3] KRIVÁ, Z.—MIKULA, K.—PEYRIÉRAS, N.—RIZZI, B.—SARTI, A.—STAŠOVÁ, O.: *3D early embryogenesis image filtering by nonlinear partial differential equations.* Medical image analysis **14** (2010), no. 4, 510–526

[4] MIKULA, K.—ŠEVČOVIČ, D.: *Evolution of plane curves driven by a nonlinear function of curvature and anisotropy*, SIAM J. Appl. Math. **61** (2001), no. 5, 1473–1501

[5] MIKULA, K.—ŠEVČOVIČ, D.: *Computational and qualitative aspects of evolution of curves driven by curvature and external force*, Computing and Visualization in Science **6** (2004), no. 4, 211–225

[6] MIKULA, K.—ŠEVČOVIČ, D.: *A direct method for solving an anisotropic mean curvature flow of plane curves with an external force.* Math. Methods in Appl. Sci. **27** (2004) (13), 1545–1565.

[7] MIKULA, K.—URBAN, J.—KOLLÁR, M.—AMBROZ, M.—JAROLÍMEK, I.—ŠIBÍK, J.—ŠIBÍKOVÁ, M.: *An automated segmentation of NATURA 2000 habitats from Sentinel-2 optical data*, Discrete and Continuous Dynamical Systems Series S (accepted).

[8] MIKULA, K.—URBAN, J.—KOLLÁR, M.—AMBROZ, M.—JAROLÍMEK, I.—ŠIBÍK, J.—ŠIBÍKOVÁ, M.: *Semi-automatic segmentation of NATURA 2000 habitats in Sentinel-2 satellite images by evolving open curves*, Discrete and Continuous Dynamical Systems Series S (accepted).

[9] PRICHARD, S. J.—SANDBERG, D. V.—OTTMAR, R. D.—EBERHARDT, E.—ANDREU, A.—EAGLE, P.—SWEDIN, K.: *Fuel characteristic classification system version 3.0: Technical documaentation.* In:*General Technical Report (GTR)*, Gen. Tech. Rep. PNW-GTR-887. Portland, OR: U.S. Department of Agriculture, Forest Service, Pacific Northwest Research Station. 79 p. DOI: https://doi.org/10.2737/PNW-GTR-887

[10] SEDINA, J.—HŮLKOVA, M.—PAVELKA, K.—PAVELKA, K. JR.: *RPAS for documentation of Nazca aqueducts*, European Journal of Remote Sensing, **52**, 174–181. (Supplement: 1 Special Issue: SI, DOI:10.1080/22797254.2018.1537684, 2019.)

[11] VIEGAS, D., ET AL.: *Slope and wind effects on fire spread.* In:*IVth International Forest Fire Conference. Coimbra (Portugal).* FFR & Wildland Fire Safety, Millpress, Rotterdam, 2002.

[12] WALKER, S.—ALSPAUGH, D.: *A Brief History of Photogrammetry.* Manual of Photogrammetry, 6th edition. ASPRS, Bethesda, Maryland, 2013.

[13] ZHANG, J. W.—HAN, G. Q.—WO, Y.: *Image registration based on generalized and mean Hausdorff distances*, Machine Learning and Cybernetics, 2005. In: *Machine Learning and Cybernetics Vol. 8*, IEEE Xplore, 2005. pp. 5117–5121.

Martin Ambroz
Karol Mikula
Department of Mathematics and
Descriptive Geometry
Faculty of Civil Engineering
Slovak University of Technology in Bratislava
Radlinského 11
810 05 Bratislava
SLOVAKIA
E-mail: martin.ambroz@stuba.sk
      karol.mikula@stuba.sk

Marek Fraštia
Marián Marčiš
Department of Surveying
Faculty of Civil Engineering
Slovak University of Technology in Bratislava
Radlinského 11
810 05 Bratislava
SLOVAKIA
E-mail: marek.frastia@stuba.sk
      marian.marcis@stuba.sk